Large-eddy simulation of dust-uplift by a haboob density current

DOI:
10.1016/j.atmosenv.2018.01.048

Document Version
Accepted author manuscript

Large-eddy simulation of dust-uplift by a haboob density current

Qian Huang[1], John H. Marsham[2], Wenshou Tian[1], Douglas J. Parker[2], Luis Garcia-Carreras[3]

1. Key Laboratory for Semi-Arid Climate Change of the Ministry of Education, College of Atmospheric Sciences, Lanzhou University, Lanzhou, China

2. School of Earth and Environment, University of Leeds, Leeds, UK

3. School of Earth, Atmospheric and Environmental Sciences, Centre for Atmospheric Science, University of Manchester, UK

Abstract

Cold pool outflows have been shown from both observations and convection-permitting models to be a dominant source of dust emissions ("haboobs") in the summertime Sahel and Sahara, and to cause dust uplift over deserts across the world. In this paper Met Office Large Eddy Model (LEM) simulations, which resolve the turbulence within the cold-pools much better than previous studies of haboobs with convection-permitting models, are used to investigate the winds that uplift dust in cold pools, and the resultant dust transport. In order to simulate the cold pool outflow, an idealized cooling is added in the model during the first 2 hours of 5.7 hour run time. Given the short duration of the runs, dust is treated as a passive tracer. Dust uplift largely occurs in the "head" of the density current, consistent with the few existing observations. In the modeled density current dust is largely restricted to the lowest, coldest and well mixed layers of the cold pool outflow (below around 400 m), except above the "head" of the cold pool where some dust reaches 2.5 km. This rapid transport

to above 2 km will contribute to long atmospheric lifetimes of large dust particles from haboobs. Decreasing the model horizontal grid-spacing from 1.0 km to 100 m resolves more turbulence, locally increasing winds, increasing mixing and reducing the propagation speed of the density current. Total accumulated dust uplift is approximately twice as large in 1.0 km runs compared with 100 m runs, suggesting that for studying haboobs in convection-permitting runs the representation of turbulence and mixing is significant. Simulations with surface sensible heat fluxes representative of those from a desert region during daytime show that increasing surface fluxes slows the density current due to increased mixing, but increase dust uplift rates, due to increased downward transport of momentum to the surface.

Key words: turbulence, haboob, density currents, dust uplift, LES

1. Introduction

Airborne mineral dust is an important component of the Earth system (Carslaw et al.,2010) and an increasing number of weather and climate models are including prognostic dust, which can improve weather prediction (Rémy et al.,2015). Dust uplift is a highly non-linear function of wind speed, usually parameterized as a threshold cubic function of the friction velocity (e.g. Gillette, 1978; Marticorena and Bergametti, 1997). This means that localized high wind-speed events can be important for dust emission (Cowie et al., 2015), making dust modeling a challenge for global models (Doherty et al., 2014).

Cold pool outflows from moist convection, generated by the evaporation, melting and sublimation of hydrometeors, are one important mechanism for generating strong winds and so dust uplift from the surface, with the dusty cold pools referred to as haboobs (Sutton, 1925; Lawson, 1971; Membery, 1985; Roberts and Knippertz, 2012). Haboobs have been observed in every major dust source region (Knippertz and Todd, 2012). They vary from barely visible dust storms produced by cumulus congestus clouds (Marsham et al., 2009) to storms hundreds of kilometers across that can

be seen clearly from space (Flamant et al., 2007; Takemi, 1999; Idso et al., 1972).

The Sahel and Sahara are the world's main dust source (Prospero et al., 2001) and haboobs are a key dust emission mechanism there (Marsham et al., 2008; Marsham et al., 2013; Allen et al., 2013; Roberts et al., 2017; Bergametti et al., 2017). Multi-day convection-permitting simulations have shown that haboobs cause around half of modeled summertime dust emission in West Africa, but that this emission is essentially missing in models that use parameterized convection (Marsham et al., 2011; Heinold et al., 2013; Pope et al., 2016) and in analyses (Largeron et al., 2015 and Roberts et al., 2017). Convection-permitting simulations (3.75 km grid-spacing) have also been used to study haboobs in the USA (Vukovic et al., 2014).

Observations show that convectively generated cold pools acting as density currents have typical depths of around 1km (Sutton, 1925; Idso et al., 1972) with some studies showing depths reaching 4 km (Bryan and Parker, 2010). There are many studies of density currents that do not consider dust uplift (Simpson, 1997; Takemi, 2005; Miller et al., 2008; Knippertz et al., 2009). These show how the low-level pressure gradient associated with the cold pool leads to strong low-level winds (see e.g. Fig 2.2 in Simpson, 1997). The density current "head" is associated with turbulent winds with less turbulent flow behind it. Kelvin-Helmholtz wave-breaking can lead to mixing between the density current and its environment (Simpson, 1972). The leading edge of the density current is composed of so-called lobes and clefts that are unsteady and shifting (Simpson, 1997, Härtel et al., 2000).

Some studies have attempted parameterization of wind gusts from convective downdrafts (Nakamura et al.,1996; Redelsperger at al.,2000; Cakmur et al., 2004) and recently for haboobs (Pantillon et al., 2015; 2016). However, despite the great importance of haboobs for global dust emission, to the best of the authors' knowledge there are no published studies of large-eddy simulations that explicitly resolve the turbulent dust-uplift in haboobs and analyse the role of

turbulence for dust emission.

In this paper we use the Met Office Large Eddy Model (LEM) to simulate idealized density currents. Our main focus is on the impacts of small-scale turbulence on the dust emission in haboobs and the effects of surface heat fluxes. We do not attempt to simulate any particular observed case, but rather use idealized simulations of a density current that has properties broadly consistent with those from observations. Section 2 describes the model used and its configuration. Section 3.1 discusses the structure and the development of the density current, dust emission and dust transport from the simulation. The scales of motion, which are responsible for dust uplift, are investigated by means of varying model horizontal grid-spacing in Section 3.2. Section 3.3 briefly examines the impact of surface sensible heat fluxes on haboobs. Section 4 contains a summary and conclusion.

2. Model setup and methods

The model used is the U.K. Met Office LEM version 2.4 (Gray and Petch, 2001). The LEM is a non-hydrostatic numerical model used to simulate a wide range of boundary-layer and cloud-scale problems. The subgrid model used in the LEM is based on the Smagorinsky-Lilly approach (Brown et al, 1994). The LEM equation set is Boussinesq and in this study the incompressible Boussinesq formulation is used. All moist processes are switched off, since the model never reached saturation and an idealized cooling is used to generate the cold pool. Two-dimensional (y-z) simulations are performed throughout this study, except for a single sensitivity study in 3D (S3D in Table 1). The domain is10km deep, and the horizontal domain length is 450 km. Horizontal grid spacing varies between 100 m and 1.0 km. A grid-spacing of 450 m is used for a standard run (S in Table 1) and runs with varying surface heat fluxes, as well as the 3-D run (Table 1). All runs used a vertically stretched grid with a minimum spacing of 0.5 m in the surface layer and a maximum of 233 m above 6000 m. Periodic lateral boundary conditions are applied, with a rigid lid at the top of the

model domain. To reduce the reflection of internal gravity waves, a Newtonian damping layer is applied above 6500 m. The model is initialized with a profile characterized by an approximately 6 km deep dry adiabatic and neutral boundary layer with a stable layer above (Fig. 1). This profile is based on an idealized version of those found in the Sahara (Cuesta et al., 2009; Garcia-Carreras et al., 2015). The profile is considerably cooler than that found in the Sahara, but that will not affect our results, as it is the temperature difference not the absolute temperature that is key to density current propagation (Simpson, 1997).

The idealized cooling used to generate the cold pool outflow is identical to that used by Orf et al. (1996). The aim is to generate a density current that was within the range of haboobs seen in observations, without attempting to represent any particular haboob event. The cooling used is,

$$Q(x,y,z;t) = \begin{cases} g(t)\cos^2(\pi R) & R \prec \frac{1}{2} \\ 0 & R \succ \frac{1}{2} \end{cases} \quad (1)$$

where R is the normalized distance from the center of cooling , given by

$$\mathrm{R} = \sqrt{\left(\frac{y-y_f}{M_y}\right)^2 + \left(\frac{z-z_f}{M_z}\right)^2} \quad (2)$$

where (y_f, z_f) is the location of the center of the forcing function and (M_y, M_z) is the horizontal/vertical half-width and

$$g(t) = \begin{cases} -\cos^2\left[\pi\left(\frac{t-0.5}{2\tau}\right)\right] & 0 \le t \prec 0.5 \\ -1 & 0.5 \le t \prec 1.5 \\ -\cos^2\left[\pi\left(\frac{t-2.0}{2\tau}\right)\right] & 1.5 \le t \prec 2.0 \end{cases} \quad (3)$$

where τ=0.5 h. A maximum cooling rate of 0.15 Ks^{-1} is used in this paper, which is comparable with the cooling rates found by Orville et al. (1989), which approach 0.1 Ks^{-1} e.g. for evaporation of rain in strong microburst cases. In all runs the cooling center is located at y_f=0 km and z_f=2 km. An

elliptical cold bubble with horizontal and vertical half-widths of 25 km (M_y) and 1.0 km (M_z) respectively, is used. The constant cooling lasts 1.0 h with a smooth ramp-up and ramp-down during 30min. Fig 1 shows the cold bubble created using the above method after 1.5 h of the model run. The difference of temperature between the cold bubble (averaged temperature) and the environment is about 9 K. As discussed in Section 3.1, this generates a density current similar to those seen in observations. The three-dimensional simulation (S3D) uses a 450 x 9 km domain. The same cooling rate used in the two-dimensional runs is applied over a 50 km long (in the y-direction) strip extending the full 9 km (in the x-direction) width of the domain, to give a setup analogous to the downdraft from linear convective systems, which dominate the precipitation in the Sahel and generate large cold pools there (Provod et al., 2016).

Based on a widely used parameterization of dust uplift by Marticorena and Bergametti (1995), the vertical dust flux in the LEM is expressed as:

$$F \propto u^{*3}(1+R)(1-R^2) \tag{4}$$

Where $R = u_T^* / u^*$, u^* is the friction velocity and u^*_T is a threshold friction velocity. Marsham et al. (2011) defined a quantity "dust uplift potential (DUP)" as,

$$DUP = \nu u^{*3}(1+u_T^*/u^*)(1-u_T^{*2}/u^{*2}) \tag{5}$$

where ν is the bare-soil fraction (bare soil everywhere is assumed in this study). A typical 10 m wind speed threshold for dust emission of 7 ms^{-1} is found by Chomette et al. (1999) in desert areas, consistent with the range shown by Cowie et al. (2014). Friction velocity u^* is output from the LEM. A threshold u_T^* for modeled dust uplift is calculated by

$$u_{T10}^* = \frac{u_T^*}{\kappa} \ln \frac{10}{z_0} \tag{6}$$

where u^*_{T10} is the 10 m wind speed threshold for dust emission of 7 ms^{-1}, z_0 the roughness length of the surface, which is 0.001 m in this study, and κ is the von Karman constant. The result is a u* threshold of 0.288 ms^{-1} for modeled dust uplift utilized in this paper. In order to only allow dust generation from the modeled density current, which is a good idealization of a cold-pool outflow, rather than from the initial impact of the cold bubble on the surface, which may be less realistic, modeled dust uplift is only allowed for $y > 60$ km. It should be pointed out that dust in this simulation does not explicitly represent dust particles with a defined size, sedimentation and a parameterization of deposition. Rather, to investigate dust generating winds in haboobs, dust is treated as a passive tracer with a surface emission flux for winds greater than the threshold. Unlike real dust, the idealized dust in the model does not fall. We note that such sedimentation would be small for the 5.7 hour simulations we consider, except for the very largest dust particles with diameters larger than 100 μm, which are usually expected to exist only in a saltation layer extending a few centimeters from the surface (although these have recently observed to be lofted higher in intense events, where turbulence can keep them aloft; Rosenberg et al., 2014). Ryder et al. (2013) illustrated that accumulation mode particles (diameter less than 3.5 microns) settle 500 m on time-scales of over a day, and coarse mode particles (4 to 30 microns) on time-scales of 2 hours to a day or more: despite this coarse mode particles are seen to travel away from the desert over the Atlantic. Therefore, except for the largest particles, in the highly turbulent active haboobs modeled here, where vertical winds are much greater than fall speeds, settling effects would be small.

Sensitivity tests with varying horizontal grid-spacing are carried out to investigate the role of different scales of motion on the dust uplift (Table 1). In order to investigate the effects of turbulence due to surface heating, as is expected in a desert during the day (Marsham et al., 2013), sensitivities to surface fluxes are studied. Heat fluxes varying from 50 to 300 Wm^{-2} are applied after the density-current formation 2.0 h into the simulations (runs F1 to F4).

3. Model results

3.1 Standard case

The modeled density current is essentially symmetric about y=0 km (center of the domain in y direction) and so Fig. 2 shows the right-hand part of the model domain for the region where uplift is allowed to occur (y > 60 km). The initial cold bubble descends to the surface and spreads as a density current. Potential temperature (black lines) clearly shows the "head" of the cold pool, which is approximately 20 km across, with waves (perhaps Kelvin Helmholtz billows) behind the "head" in Fig. 2a, which then grow to a larger amplitude in Fig. 2b. There is ascent of air at the leading edge of the cold pool with descent 10 to 20 km behind.

Dust amounts in the "head" are more than double those in the "tail" (Fig. 2). Dust is largely trapped in the lowest, coldest and well-mixed layer of the density current, up to around 400 m in the head and 200 m in the "tail". The 400 m deep dust layer of the head is shallower than the haboob shown in Flamant et al. (2007), which reaches up to around 1 km, but is within the range of depths of haboob dust layers observed by Miller et al. (2008), which vary from 300 m to 500 m. The simulations show that low amounts of dust (mass-fraction of dust is about 2.5, approximately ten times lower than in the head) reaching altitudes of up to 2.5 km (Fig. 2c) where they are swept back over the density current (Fig. 2d). This plume of low dust amounts is initially lifted by the ascent forced above the main cold pool head to around 2.5 km (Fig 2c), before descending to around 1 km (Fig 2d). This dust is in relatively cold air, suggesting it is mixed out of the main cold dusty density current. Lidar-derived reflective measurements in Flamant et al. (2007) (Fig. 9b) showed that the elevated lidar-derived reflectivity values were found behind the dust front leading edge above the main haboob (at latitudes of 16 to 16.3°N and heights of between 2 km and 4 km). It was hypothesized that it was possible for dust to be injected from the main haboob into this neutrally stratified layer above, again showing consistency between our idealized simulation and observations. Rapid transport to high altitudes over the main density current is likely to be

particularly important for the largest particles that will fall out fastest from low levels, but can persist for much longer if quickly transported to higher in the boundary layer. Therefore the rapid transport of low concentrations of dust to significantly above the depth of the main dust layer may contribute to recent observations of giant particles persisting 12 hours after a haboob event (Ryder et al., 2013).

Fig. 3 shows Hovmöllers of potential temperature and wind speed at the lowest model level for the standard run. Fig. 3a shows that the leading edge of the cold pool has an approximately constant velocity of 16.7 ms^{-1} with the head approximately 10 K cooler than the environment. Observations of strong cold pool in the Sahara and Sahel show that the range of temperature decreases associated with cold pools is from 2 K to 14 K and the moving speed of leading edges varies from 3 ms^{-1} to 22 ms^{-1} (Flamant et al., 2007; Marsham et al., 2013; Provod et al., 2016). These are consistent with results from the USA (Engerer et al., 2008). It illustrates that the characteristics of the idealized cold pool simulated using LEM are broadly consistent with observed cases. The strongest near-surface winds of around 13.5 ms^{-1} are present in the "head" (Fig. 3b), with weaker winds behind and wind velocities well above the surface and in the head exceeding the velocity of the density current (not shown). Past observational studies show that maximum near-surface wind values between 4 ms^{-1} and 22 ms^{-1} are found in the "head" of cold pools (Sutton, 1925; Freeman, 1952; Miller et al., 2008; Provod et al., 2016) so the idealized cold pool is approximately in the middle of this range seen in observations. Fig. 3a also shows that it is colder in the "tail" than in the "head" of cold pools due to relative strong mixing with the ambient warm air occurring in the "head", again consistent with observations (Marsham et al., 2013).

Fig. 4a and 4b show Hovmöllers of the dust uplift potential and total dust integrated over the vertical column from the standard run, respectively. Fig. 4a shows that winds above our threshold for dust emission are largely found within 20 km of the leading edge of the cold pool, i.e. in the

"head" of the density current, and therefore high values of DUP are restricted to this region, and last around one hour at any fixed point. DUP values in the "tail" are about 6 times lower than those in the "head" (comparable with observations from the Sahara shown in Fig. 14b of Marsham et. al., 2013). Figure 4b shows that total column dust loads in the "head" are around triple those in the "tail". It is likely that the difference in dust loadings between the "head" and the "tail" would be even larger if sedimentation were taken into account.

3.2 Effects of model resolution

Fig. 5 shows the same results as Fig. 2, but from the run R2 (200 m grid-spacing), rather than run S with a 450 m grid-spacing. The figure shows that turbulence is strengthened both in the cold pool "head" and behind it, with more obvious and smaller scale waves (perhaps Kelvin-Helmholtz waves) behind the "head" (Fig. 5a compared with Fig. 2a). The height of dust transport reaches about 1.0 km in the "head" and 500 m in the "tail", similar to the standard run S, but with lower overall dust amount in the haboob. The propagation speed of the cold pool in Fig. 5 is lower than that in Fig. 2 (14.6 ms^{-1} compared with 16.7 ms^{-1}). It is also noted that the width of the cold pool "head" becomes smaller as the grid-spacing decreases to 200 m.

To examine the characteristics of cold pools simulated using different resolutions, it is useful to examine the time-evolution of surface potential temperature. Hovmöller diagrams of potential temperatures from runs with different horizontal grid-spacing (not shown) show that the cold pool becomes colder as the grid-spacing increases. For the different resolution runs in Table 1, Table 2 compares the mean propagation speed of the cold pools, the mean temperature contrasts across their leading edges, and their maximum and mean DUPs. Table 2 shows that mean temperature differences across the cold pool leading edge increases with grid-spacing, with values of about 7.6 K, 12.8 K, 16.7 K and 23.8 K with grid-spacings of 100 m, 300 m, 500 m and 1.0 km, respectively. This is presumably because cold pools warm more in higher resolution runs due to better resolved

turbulent mixing with the surroundings. This leads to a decrease of the propagation speed of cold pools in the higher resolution runs. The cold pool moves at a speed of 15.3 ms^{-1} with a grid-spacing of 100 m, increasing to 16.0 ms^{-1}, 16.7 ms^{-1}, 23.6 ms^{-1} when the grid-spacing increases to 300 m, 500 m and 1.0 km, respectively (Table 2), consistent with the colder and denser density currents at the coarser grid spacing.

Fig. 6 is the Hovmöller diagram of the total dust uplift potential from different horizontal grid-spacing runs. It shows that the resolved small eddies from the high resolution runs (Fig. 6a) locally increase the DUP behind the cold pool "head", due to turbulence locally increasing the strength of surface wind speeds. However, high DUP values are more widespread in the coarse resolution runs (Fig. 6c and Fig. 6d). Table 2 shows that the maximum DUPs are relative large in the high resolution runs, but with larger mean DUPs in the coarse resolution runs. Total accumulated DUPs (Fig.7) show lower resolution runs give around twice as much DUP (run R8) as higher resolution runs (run R1). This shows that the locally increased DUP from better resolved turbulence in high resolution runs is not compensating for greater DUP from the stronger cold pools in lower resolution runs. It should be noted that although the cold pool temperature deficit is monotonic with resolution, and propagation speed is almost monotonic (Table 2), values of DUP are less so (Table 2 and Figure 7). It is not clear what causes this: one hypothesis is that once the horizontal grid-spacing becomes comparable with the depth of the density current head this inhibits the turbulence that causes high winds leading to the temporary decrease in accumulated DUP seen at grid spacings of 600 m and 750 m in Figure 7.

The differences in the PDFs of surface wind speed, surface potential temperature and total DUP between the 2D and 3D versions of the standard case (S and S3D) are small (not shown), although there is more small-scale turbulence created in the 3D run. Table 2 shows that difference between 2D and 3D runs are generally small compared with those from changing grid spacing in a 2D run.

This suggests the inferences we make from the 2D runs are applicable to 3D systems.

3.3 Effects of surface heat flux

Effects of surface heat fluxes on the evolution of cold pools have been studied by Ross et al. (2004) and Gentine et al. (2016), but how a surface heat flux alters the dust uplift in cold pools has not been addressed. To investigate the effects of buoyancy driven turbulence on the modeled haboob dust uplift, Fig. 8 shows Hovmöller diagrams of potential temperature differences for four runs with different surface heat fluxes and the standard run, which has no surface heat flux. As expected the surface heating warms the cold pool (also in Table 2, temperature differences decrease from 15.0 K to 14.4 K with surface heat flux increasing from 50 Wm^{-2} to 300 Wm^{-2}), both directly, and also through increased mixing of environmental air into the cold pool. This leads to the cold pool "head" temperature increasing by about 2 K (Fig. 8a) to 15 K (Fig. 8d) compared with the standard run, with temperatures in the "tail" increasing by about 5 K to 20 K. Fig.9 shows that surface wind speeds behind the cold pool's "head" increase with surface heat fluxes increasing. The maximum surface wind differences (from 2 h to 5 h) are 2.3 ms^{-1}, 3.0 ms^{-1}, 3.9 ms^{-1} and 4.6 ms^{-1} with surface heat fluxes of 50 Wm^{-2} (Fig. 9a), 100 Wm^{-2} (Fig. 9b), 200 Wm^{-2} (Fig. 9c) and 300 Wm^{-2} (Fig. 9d), respectively. The heat fluxes increase the downward transport of momentum, thus increasing near-surface winds. The decrease in surface wind speeds at the leading edge of the cold-pool "head" from increasing the surface heating, as shown in Figure 1, results from the cold pools moving more slowly due to the stronger turbulent mixing.

In order to examine the effects of turbulence in the density current on dust uplift, Fig. 10 shows total DUP (for $y > 60$ km) as a function of surface heat flux. A surface heat flux of 300 Wm^{-2} increases maximum DUP from 75 to 120 m^3s^{-3}, but as noted leads to a warmer density current. This would eventually lead to a less long-lived haboob, and perhaps less total dust uplift, but computational constraints prevented domains that were sufficiently large to investigate this.

However, since dust uplift is highly non-linear with much stronger uplift for high winds, it might be expected that for a more rapid mixing of any given momentum source to the surface would increase total uplift. This increased uplift from heating is consistent with the peak in surface winds from haboobs after sunrise observed in Allen et al. (2013) and seen in convection-permitting runs by Heinold et al. (2013). It is interesting to note that even after 5 hours the behavior in the different simulations continue to diverge, suggesting sensible heat flux differences can have a large impact on the long term evolution of cold pools.

4. Summary and conclusions

Haboobs are crucial to the seasonal cycle of dust emission in the Sahara and Sahel and produce high-impact dust events (Marsham et al., 2008; Marsham et al., 2013; Allen et al., 2013; Bergametti et al., 2017). They are essentially missing in global models that use parameterized convection (Marsham et al., 2011), but convection-permitting simulations with grid-spacings of around 1.5 to 4 km have been used to study specific events and their overall contribution to dust uplift and to develop parameterizations (Marsham et al., 2011;Heinold et al., 2013;Vukovic et al., 2014; Pantillion et al., 2015, 2016). Here, large-eddy simulations, which resolve the flow inside the density current much better than these convection-permitting studies, have been performed to investigate the structure and development of dust uplift and transport in an idealized haboob density current, as well as the effects of surface fluxes and model resolution on haboob dust uplift.

In the simulations most high winds and dust uplift occur in the density current "head", consistent with the limited observations available. Dust is largely restricted to the lowest and coldest layer of the density current (below 500 m), with the dust layer in the density-current "head" deeper than that in the "tail" behind. In the region of the "head" some dust is also mixed into the environment, reaching altitudes of 2.5km. This transport of dust into higher altitudes is expected to significantly affect its subsequent transport and evolution.

Decreasing the model horizontal grid-spacing from 1.0 km to 100 m resolves more small-scaled turbulence and enhances mixing, increasing the temperature of the cold pool and reducing the cold-pool propagation speed. A 3D simulation of a 9 km strip (in the x direction) presents very similar results to the equivalent 2D simulation. For runs using horizontal grid spacings from 100 m to 1.0 km, the difference in total accumulated dust uplift reaches a factor of two. While this difference shows that better resolving turbulence has a strong impact on simulated dust uplift, there are other large sources of uncertainty, even when using kilometer-scale numerical weather prediction (NWP) models. Considering these other uncertainties, such as the models' ability to represent the parent moist convection and associated diabatic cooling, as well as the land-surface characteristics and dust uplift process itself, suggests that the resolution of the cold pools is not a fundamental limit of such studies, but future research should ideally address the role of the representation of turbulence and mixing in cold pools in convection-permitting models.

Imposing surface heat fluxes representative of a desert during daytime increases downward mixing of high winds towards the surface, increasing dust uplift rates by a factor of up to 1.8. Such heating and increased mixing warms the density current. Differences of sensible heat flux, however, can have a large impact on the long term evolution of cold pools. This may eventually lead to less total uplift with higher surface heating due to reductions in the haboob's lifetime, but due to computational constraints this could not be investigated.

The results presented here show for the first time the effects of resolving small-scale turbulence by large-eddy simulation on dust uplift and transport within cold pools. The results suggest that it is reasonable to continue to use convection-permitting models to develop haboob parameterizations, but resolution of eddies is key for modeling the peak winds within any haboob. This is an idealized simulation of one 'typical' cold pool. More work is therefore needed to understand the implications of these results for the broad range of cold pools that occur in reality. Given the extremely poor rep-

resentation of haboobs by global models the results show that accounting for turbulence within haboobs is of secondary importance, although in the long term this should be included, especially for convection-permitting models, where haboobs are explicitly captured.

Acknowledgments This work has been supported by the Science of Foundations of China (41775013, 41575038 and 41475095). Marsham and Parker are supported by the NERC SWAMMA project (NE/L005352/1). Parker is also supported by a Royal Society Wolfson Research Merit Award. Q.H. thanks the U.K. Met Office for Large Eddy Model support during this study. We would like to thank two anonymous reviewers whose comments have improved the quality of the manuscript.

References

Allen, C.J.T., Washington, R., Engelstaedter, S., 2013. Dust emission and transport mechanisms in the central Sahara: Fennec ground-based observations from Bordj Badji Mokhtar June2011. J. Geophys. Res. 118, 6212–6232.

Bergametti, G., Marticorena, B., Rajot, J.L., Chatenet, B., Féron, A., Gaimoz, C., Siour, G., Coulibaly, M., Kone, I., Maman, A., Zakou, A. 2017. Dust uplift potential in the central Sahel: An analysis based on 10 years of meteorological measurements at high temporal resolution. J. Geophys. Res. 122, 12,433–12,448.

Brown, A.R., Derbyshire, S.H., Mason, P.J., 1994. Large-eddy simulation of stable atmospheric boundary layers with a revised stochastic subgrid model. Quart. J. Roy. Meteorol. Soc., 120, 1485–1512.

Bryan, G.H., Parker, M.D., 2010. Observations of a squall line and its near environment using high-frequency rawinsonde launches during vortex2. Mon. Weather Rev. 138,4076–4097.

Cakmur, R.V., Miller, R.L., Torres, O., 2004.Incorporating the effect of small-scale circulations upon dust emission in an atmospheric general circulation model. J. Geophys. Res. 109, 1728–

1737.

Carslaw, K.S., Bucher, O., Spracklen, D.V., Mann, G.W., Rae, J.G.L.,Woodward, S., Kulmala, M., 2010. A review of natural aerosol interactions and feedbacks within the earth system. Atmos. Chem. Phys.10, 1701–1737.

Chomette, O., Legrand, M., Marticorena, B., 1999.Determination of the wind speed thresh old for the emission of desert dust using satellite remote sensing in the thermal infrared. J. Geophys. Res. 104, 31,207–31,215.

Cowie S.M., Knippertz, P., Marsham, J.H., 2014.A climatology of dust emission events from northern Africa using long-term surface observations. Atmos. Chem. Phys. 14, 8579–8597.

Cowie S.M., Knippertz, P., Marsham, J.M., 2015.The importance of rare, high-wind events for dust uplift in northern Africa. Geophys. Res. Letts.42, 8208–8215.

Cuesta, J., Marsham J.H., Parker, D.J., Flamant, C., 2009.Dynamical mechanisms controlling the vertical redistribution of dust and the thermodynamic structure of the west Saharan atmospheric boundary layer during summer. Atmos. Sci. Letts. 10, 34–42.

Doherty M., Riemerand, N., Hameed, S., 2014.Role of the convergence zone over West Africa in controlling Saharan mineral dust load and transport in the boreal summer.TellusB.66, 759–763.

Engerer, N.A., Stensrud, D.J., Coniglio, M.C., 2008. Surface characteristics of observed cold pools. Mon. Wea. Rev., 136, 4839–4849.

Flamant, C., Chaboureau, J.P., Parker, D.J., Taylor, C.M., Cammas, J.P., Bock, O., Timouk, F., Pelon, J., 2007. Airborne observations of the impact of a convective system on the planetary boundary layer thermodynamics and aerosol distribution in the intertropical discontinuity region of the west African monsoon. Quart. J. Roy. Meteor. Soc. 133, 1175–1189.

Freeman, L.H., Dust storms of the Anglo-Egyptian Sudan, 1952. Meteor. Report 2, 11, Great Britain Met. Office Publication, 22pp.

Garcia-Carreras L., Parker, D.J., Marsham, J.H., Rosenberg, P.D., Brooks I.M., Lock A.P., Maren-

co, F., Mcquaid, J.B., Hobby, M., 2015. The turbulence structure and diurnal growth of the Saharan atmospheric boundary layer. J. Atmos. Sci. 72, 693–713.

Gentine, P., Garelli, A., Park, S.B., Nie, J., Torri, G., Kuang, Z., 2016. Surface heat fluxes underneath cold pools. Geophys. Res. Lett., 43, 874–883.

Gillette, D., 1978.A wind tunnel simulation of the erosion of soil: Effect of soil texture, sand blasting, wind speed, and soil consolidation on the dust production. Atmos. Environ. 12, 1735–1743.

Gray, M.E.B., Petch, J., 2001. Version 2.3 of the Met. Office large eddy model. The Met. Office, Exeter, UK.

Härtel, C., Meiburg, E., Necker, F., 2000. Analysis and direct numerical simulation of the flow at a gravity-current head, part 2: the lobe and cleft instability. J. Fluid Mech. 418, 213–229.

Heinold, B., Knippertz, P., Marsham, J.H., Fiedler, S., Dixon, N.S., Schepanski, K., Laurent B., Tegen, I., 2013.The role of deep convection and nocturnal low-level jets for dust emission in summertime west Africa: Estimates from convection- permitting simulations. J. of Geophys. Res. 118, 4385–4400.

Idso, S.B., Ingram, R.S., Pritchard, J.M., 1972. An American haboob. Bull. Am. Met. Soc. 53, 930–935.

Knippertz, P., Trentmann, J., Seifert, A., 2009. High-resolution simulations of convective cold pools over the northwestern Sahara. J. Geophys. Res. 114, 10638–10654.

Knippertz, P., Todd, M.C., 2012. Mineral dust aerosols over the Sahara: Meteorological controls on emission and transport and implications for modeling. Reviews of Geophysics. 50, 140–147.

Largeron, Y., Guichard, F., Bouniol, D., Couvreux, F., Kergoat, L., Marticorena, B., 2015. Can we use surface wind fields from meteorological reanalyses for Sahelian dust emission simulations? Geophys. Res. Letts.42, 2490–2499.

Lawson, T.J., 1971.Haboob structure at Khartoum.Weather.26, 105–112.

Marsham, J.H., Parker, D.J., Grams, C.M., Johnson, B., Grey, W.M.F., Ross, A.N., 2008. Observa-

tions of mesoscale and boundary-layer scale circulations affecting dust transport and uplift over the Sahara. Atmos. Chem. Phys. 8, 6979–6993.

Marsham, J.H., Grams, C.M., Mohr, B., 2009. Photographs of dust uplift from small-scale atmospheric features. Weather. 64, 180–181.

Marsham, J.H., Knippertz, P., Dixon, N.S., Parker, D.J., Lister, G.M.S., 2011. The importance of the representation of deep convection for the modeled dust-generating winds over west Africa during summer. J. Geophys. Res. Letts. 38, 239–255.

Marsham, J.H., Hobby, M., Allen, C.J.T., Banks, J.R., Bart, M., Brooks, B.J., Cavazos-Guerra, C., Engelstaedter, S., Gascoyne, M., Lima, A.R., Martins, J.V., McQuaid, J.B., O'Leary, A., Ouchene, B., Ouladichir, A., Parker, D.J., Saci, A., Salah-Ferroudj, M., Todd, M.C., Washington, R., 2013.Meteorology and dust in the central Sahara: Observations from Fennec supersite-1 during the June 2011 Intensive Observation Period. J. Geophys. Res. Atmos. 118, 4069–4089.

Marticorena, B., Bergametti, G., 1995. Modeling the atmospheric dust cycle: 1. Design of a soil-derived dust emission scheme. J. Geophys. Res. 100, 16,415–16,430.

Marticorena, B., Bergametti, G., Aumont, B., Callot, Y., N'Doum, C., Legrand, M., 1997. Modeling the atmospheric dust cycle: 2-simulations of Saharan dust sources. J. Geophys. Res., 102, 4387–4404.

Membery, D., 1985. A gravity-wave haboob? Weather. 40, 214–221.

Miller, S.D., Kuciauskas, A.P., Liu, M., Ji, Q., Reid, J.S., Breed, D.W., Walker, A.L., Mandoos, A. A., 2008.Haboob dust storms of the southern Arabian peninsula. J. Geophys. Res. 113, 411–437.

Nakamura, K., Kershaw, R., Gait, N., 1996.Prediction of near-surface gusts generated by deep convection. Meteor. Appl. 3, 157–167.

Orf, L.G., Anderson, J.R., Straka, J.M., 1996. A three-dimensional numerical analysis of colliding microburst outflow dynamics. J. Atmos. Sci. 53, 2490–2511.

Orville, H.D., Farley, R.D., Chi, Y-C, Kopp, F.J., 1989. The primary cloud physics mechanisms of microburst formation. Atmos. Res., 24, 343–357.

Pantillon F., Knippertz, P., Marsham, J.H., Birch, C.E., 2015. A parameterization of convective dust storms for models with mass-flux convection schemes. J. Atmos. Sci. 72, 2545–2561.

Pantillon F., Knippertz, P., Marsham, J.H., Panitz, H., Bischoff-Gauss, I., 2016. Modelling haboob dust storms in large-scale weather and climate models. J. Geophys. Res. Atmos.121, 2090–2109.

Pope, R.J., Marsham, J.H., Knippertz, P., Brooks, M.E., Roberts, A.J., 2016. Identifying errors in dust models from data assimilation. Geophys. Res. Letts.43, 9270–9279.

Prospero J.M., Ginoux, P., Torres, O., Nicholson, S., Gill, T., 2001. Environmental characterization of global sources of atmospheric soil dust identified with the NIMBUS7 Total Ozone Mapping Spectrometer (TOMS) absorbing aerosol product. Rev. Geophys. 40, 2011–2020.

Provod, M., Marsham, J.H., Parker, D.J., Birch, C., 2016. A characterization of cold pools in the West African Sahel. Mon. Wea. Rev. 144, 1923–1934.

Redelsperger, J. L., Guichard, F., Mondon, S., 2000.A parameterization of mesoscale enhancement of surface fluxes for large-scale models. J. Climate, 13, 402–421.

Rémy S., Benedetti, A., Bozzo, A., Haiden, T., Jones, L., Razinger, M., Flemming, J., Engelen, R.J., Peuch, V.H., Thepaut, J.N., 2015. Feedbacks of dust and boundary layer meteorology during a dust storm in the eastern Mediterranean. Atmos. Chem. Phys. 15, 12909–12933.

Roberts A., Marsham, J.H., Knippertz, P., Parker, D.J., Bart, M., Garcia-Carreras, L., Hobby, M., McQuaid, J.B., Rosenberg, P.D., Walker, D., 2017. New Saharan wind observations reveal substantial biases in analyzed dust-generating winds. Atmos. Sci. Letts., 18, 366-372.

Rodwell, M.J., Jung, T., 2008. Understanding the local and global impacts of model physics changes: an aerosol example. Quart. J. Roy. Meteor. Soc. 134, 1479–1497.

Rosenberg, P.D., Parker, D.J, Ryder, C. L., Marsham, J. H., Garcia-Carreras, L., Dorsey, J. R.,

Brooks, I.M., Dean, A.R., Crosier, J., McQuaid, J.M., 2014. Quantifying particle size and turbulent scale dependence of dust flux in the Sahara using aircraft measurements. J. Geophys. Res. Atmos.119, 7577–7598.

Ross, A.N., Tompkins, A.M., Parker, D.J., 2004. Simple models of the role of surface fluxes in convective cold pool evolution, J. Atmos. Sci., 61, 1582–1595.

Ryder, C.L., Highwood, E.J., Lai, T.M., Sodemann, H., Marsham, J.H., 2013. Impact of atmospheric transport on the evolution of microphysical and optical properties of Saharan dust. Geophys. Res. Letts. 40, 2433–2438.

Simpson, J., 1997. Gravity currents in the environment and the laboratory.1 John Wiley, Halsted, U.K., 244 pp.

Simpson, J.E., 1972. Effects of the lower boundary on the head of a gravity current. J. Fluid Mech. 53, 759–768.

Sutton, L.J., Inst, F., 1925. Haboobs. Quart. J. Roy. Meteor. Soc. 51, 25–30.

Takemi, T., 1999.Structure and evolution of a severe squall line over the arid region in northwest China, Mon. Wea. Rev. 127, 1301–1309.

Takemi, T., 2005. Explicit simulations of convective-scale transport of mineral dust in severe convective weather. J. Roy. Meteorol. Soc. of Japan. 83A, 187–203.

Vukovic A., Vujadinovic, M., Pejanovic, G., Andric, J., Kumjian, M.R., Djurdjevic, V., Dacic, M., Prasad, A.K., El-Askary, H.M., Paris, B.C., Petkovic, S., Nickovic, S., Spring, W.A., 2014. Numerical simulation of “an American haboob”. Atmos. Chem. Phys. 14, 3211–3230.

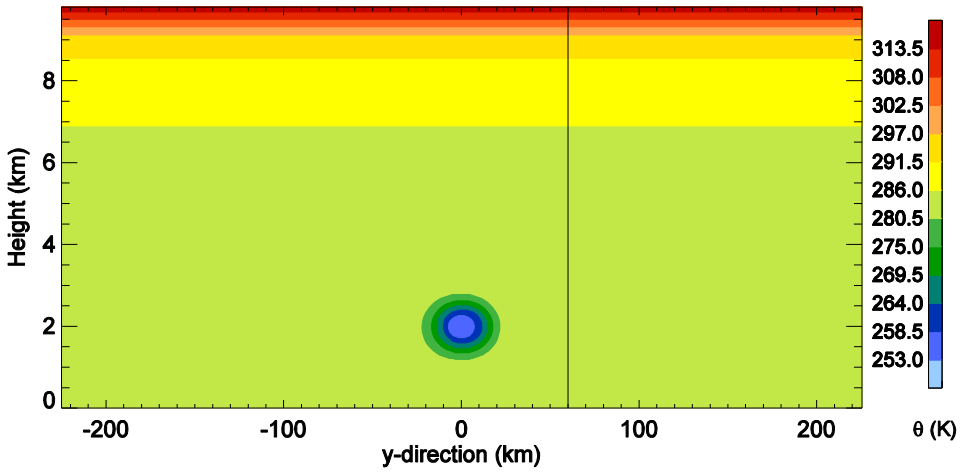

Fig. 1.Potential temperature (K) from the standard run at 1.5 h. The area to the right of the black line (y > 60 km) is shown in subsequent figures.

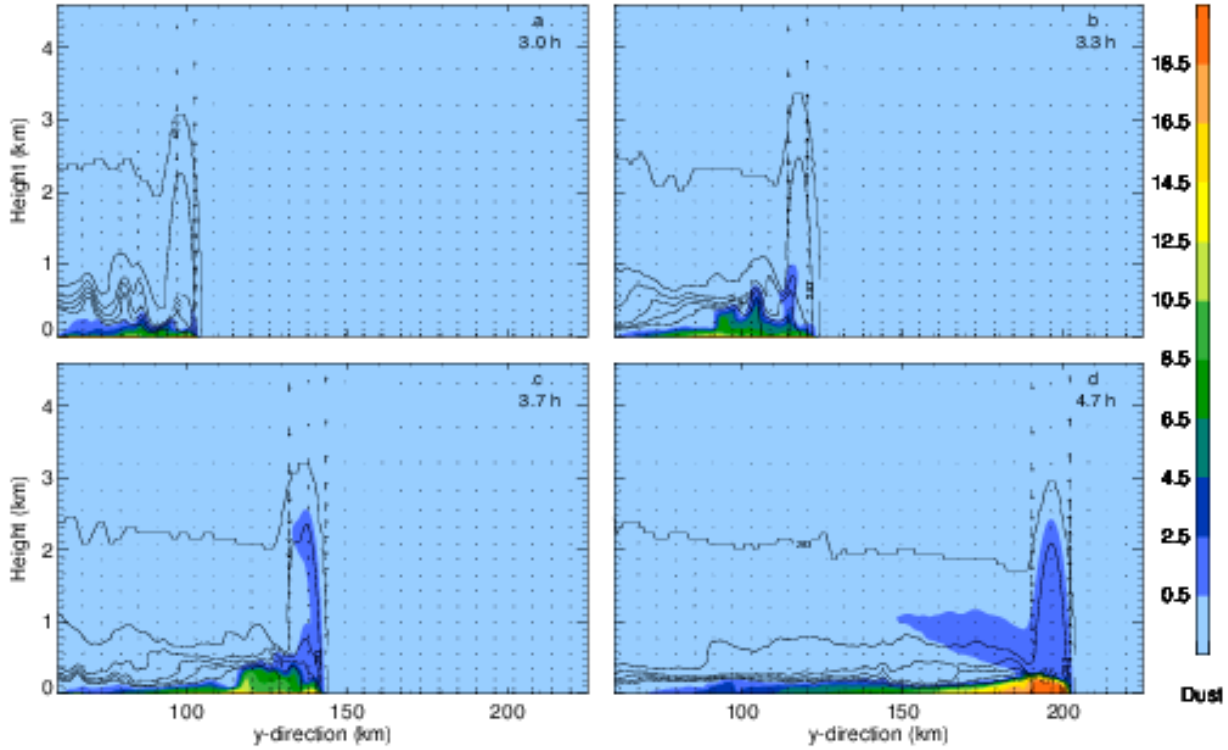

Fig. 2. Potential temperature (black lines, in order to show the stratification inside the cold pool clearly, contoured at 268K, 271K, 274K, 275 K, 278 K, 281 K and 283 K), dust (colored, arbitrary units) and wind vectors (black arrows) from the standard run at (a) 3.0 h (b) 3.3 h, (c) 3.7 h, (d) 4.7 h.

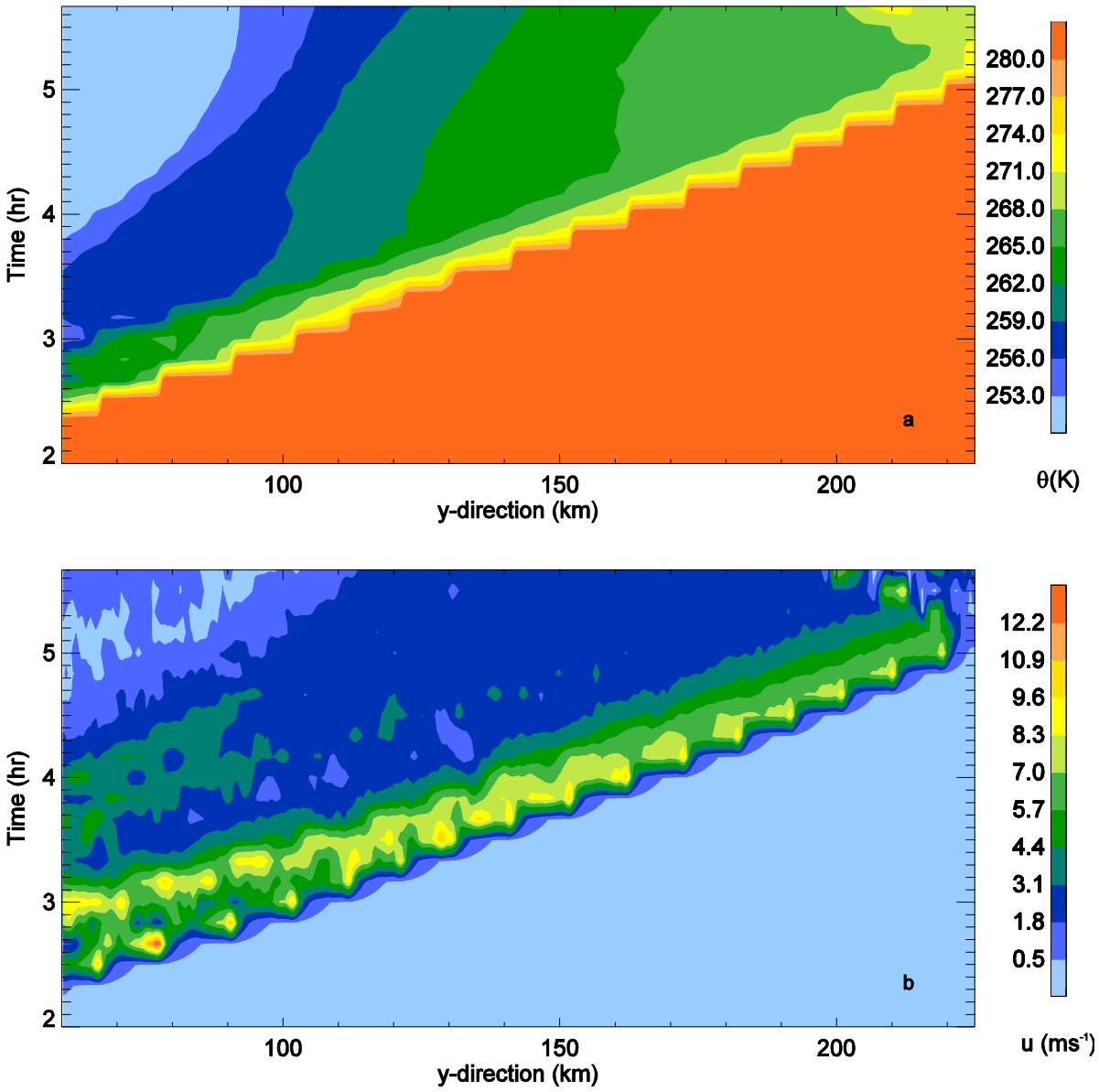

Fig. 3.Hovmöller diagrams of potential temperature (a) and wind speed (b) at the lowest model level (0.5 m AGL, above ground level) from the standard run. The discrete time-intervals with which diagnostics must be output from the model give the steps in Hovmöller plots.

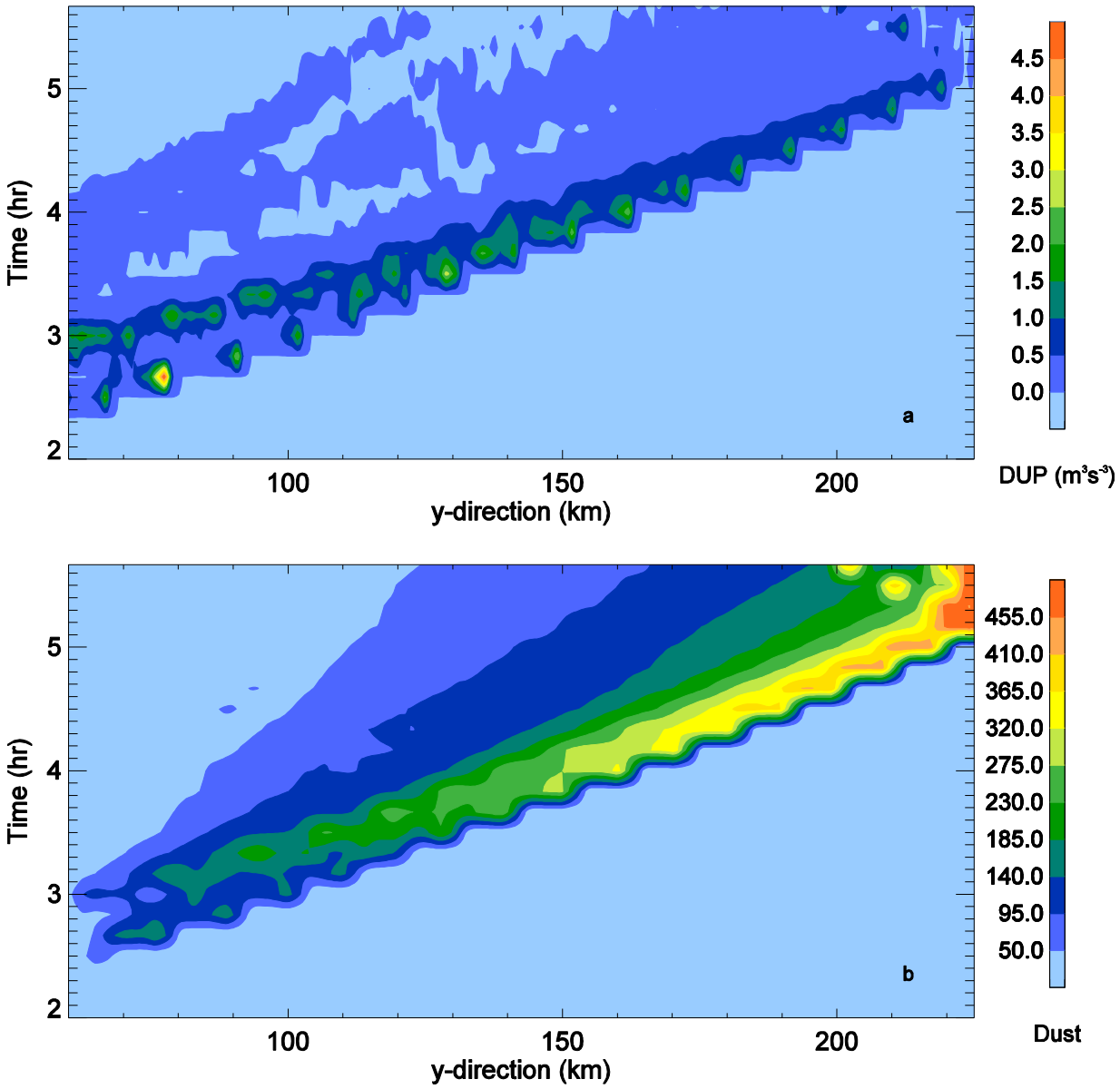

Fig. 4.Hovmöller diagrams of dust uplift potential (a) and total dust (y >60 km) integrated over the vertical column (b) from the standard run (S). The discrete time-intervals with which diagnostics must be output from the model give the steps in Hovmöller plots.

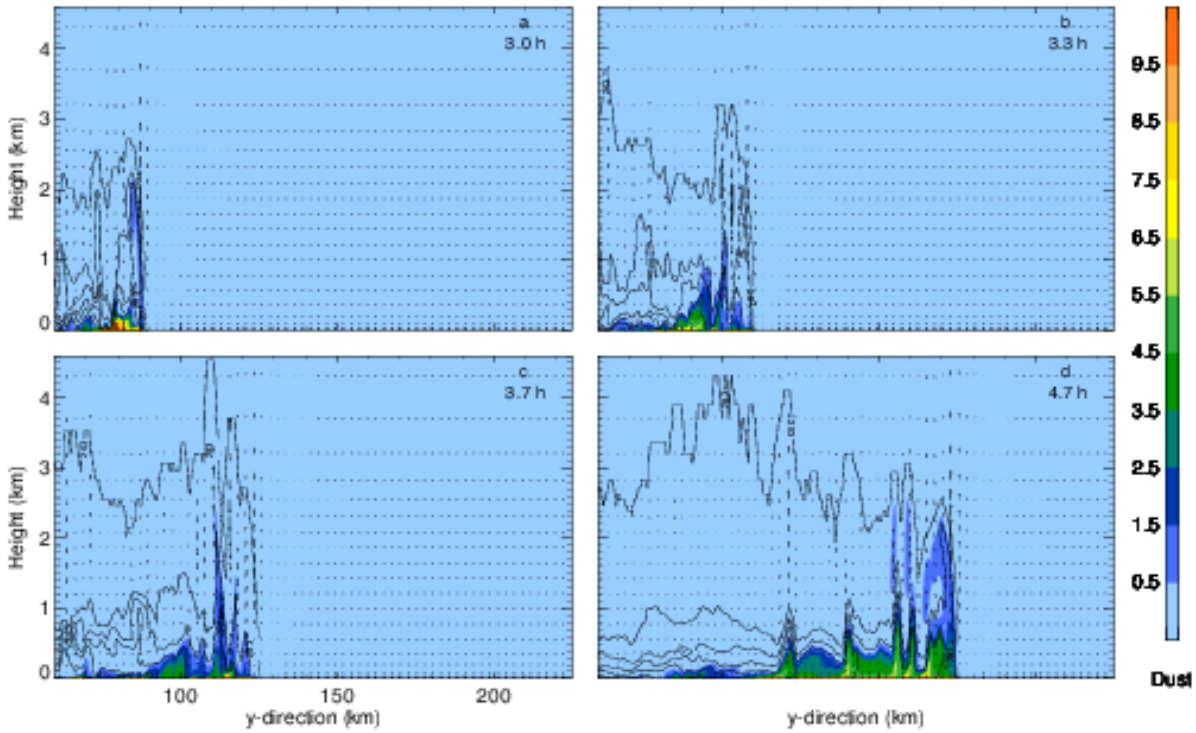

Fig. 5.Same as Fig. 2 but for run R2 (with a resolution of 200 m). Note the different scale compared to Fig. 2.

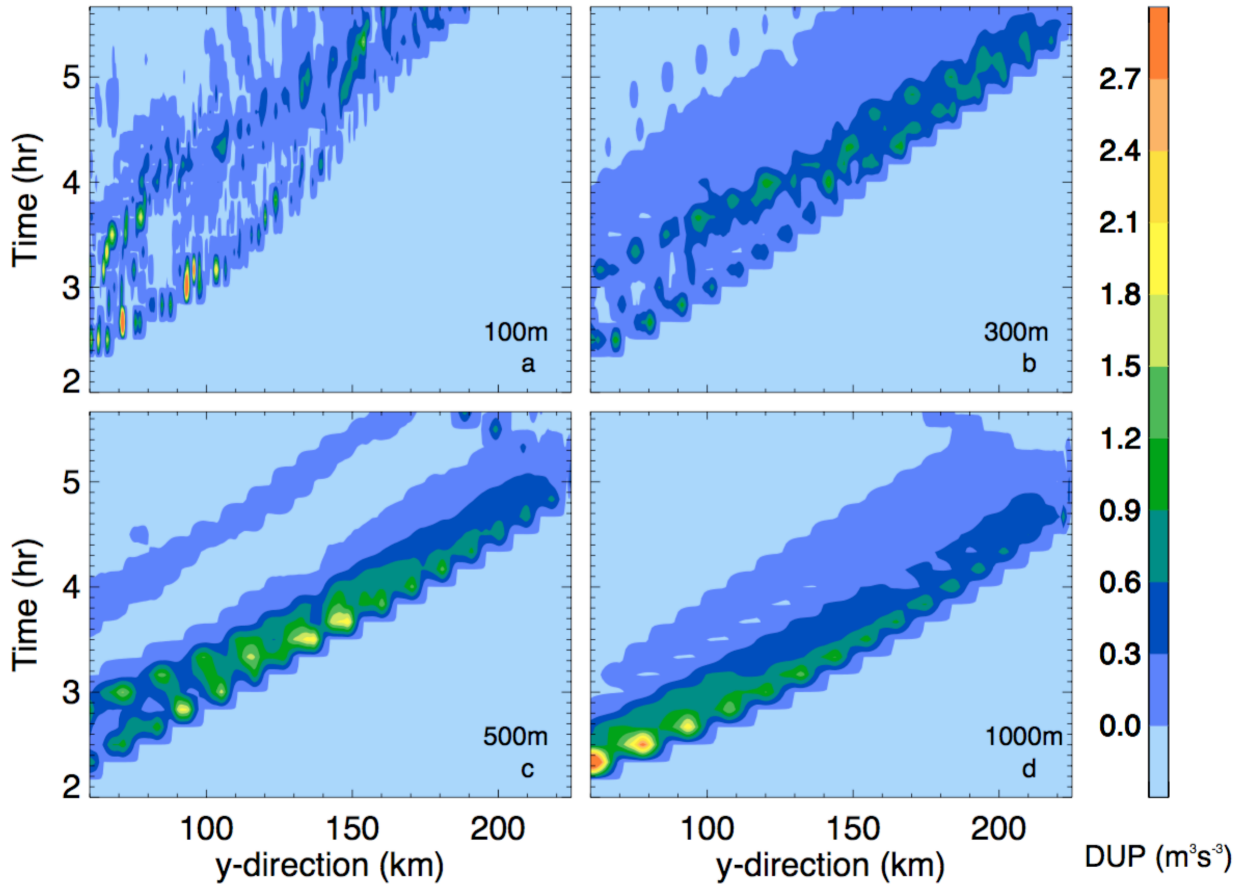

Fig.6.Hovmöller diagrams of the total dust uplift potential from runs with varying horizontal grid-spacings (Grid spacings are labeled on the panels) .

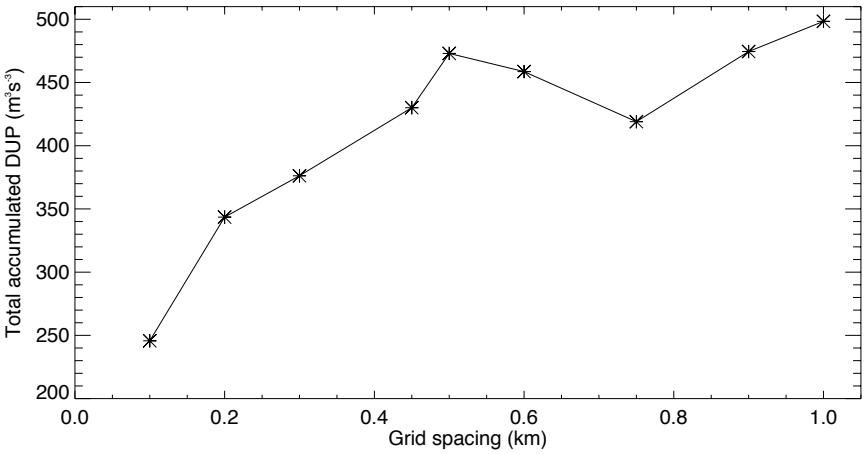

Fig. 7.Time (from 0 s to 5.7 h) and space (for y > 60 km) accumulated DUP from runs with varying grid-spacings.

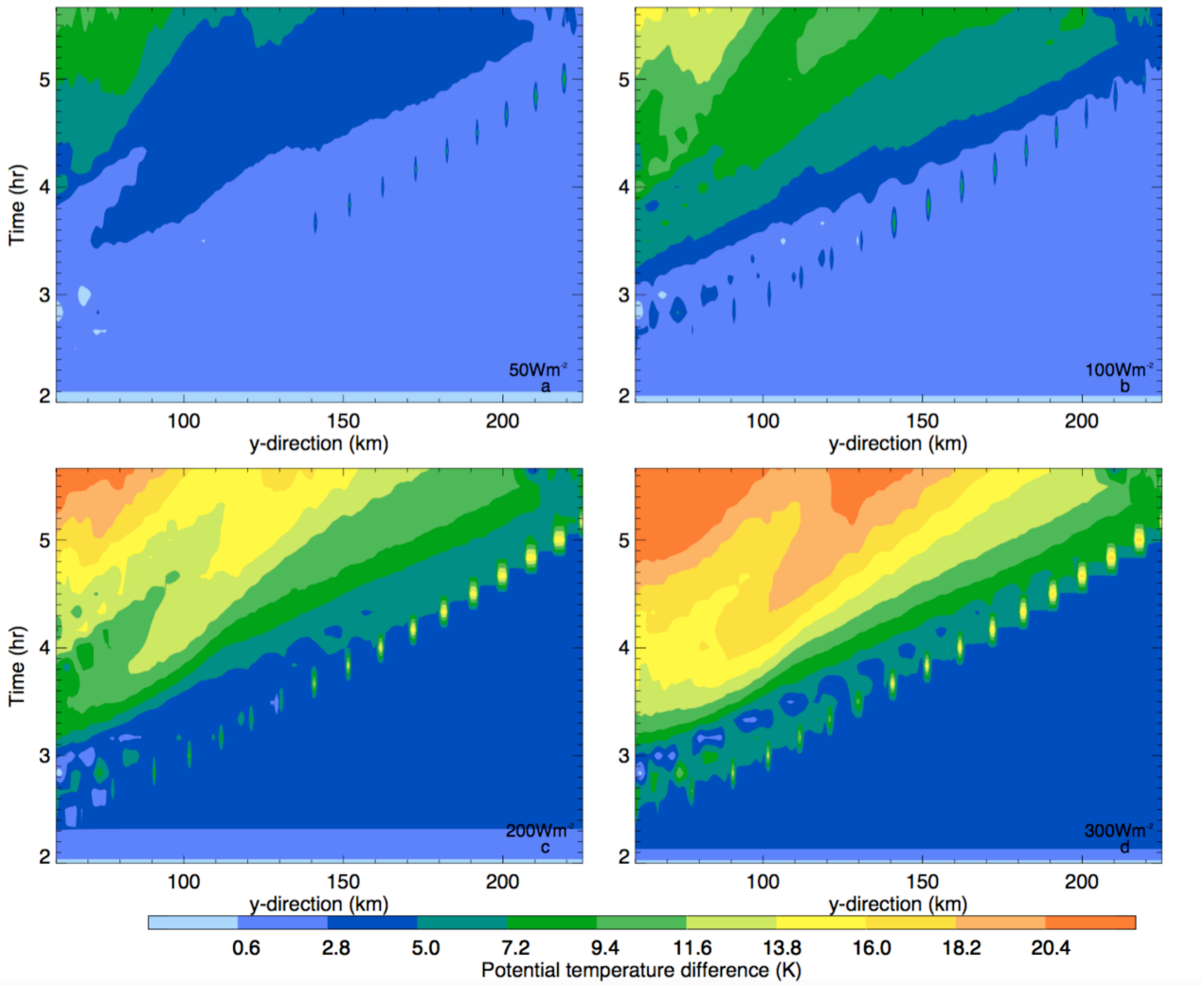

Fig. 8.Hovmöller diagrams of the potential temperature difference at the surface layer (0.5 m AGL) between the run (a) 50 Wm^{-2} (F1), (b) 100 Wm^{-2} (F2), (c) 200 Wm^{-2} (F3) and 300 Wm^{-2} (F4) surface heat flux and the standard run （S）, respectively.

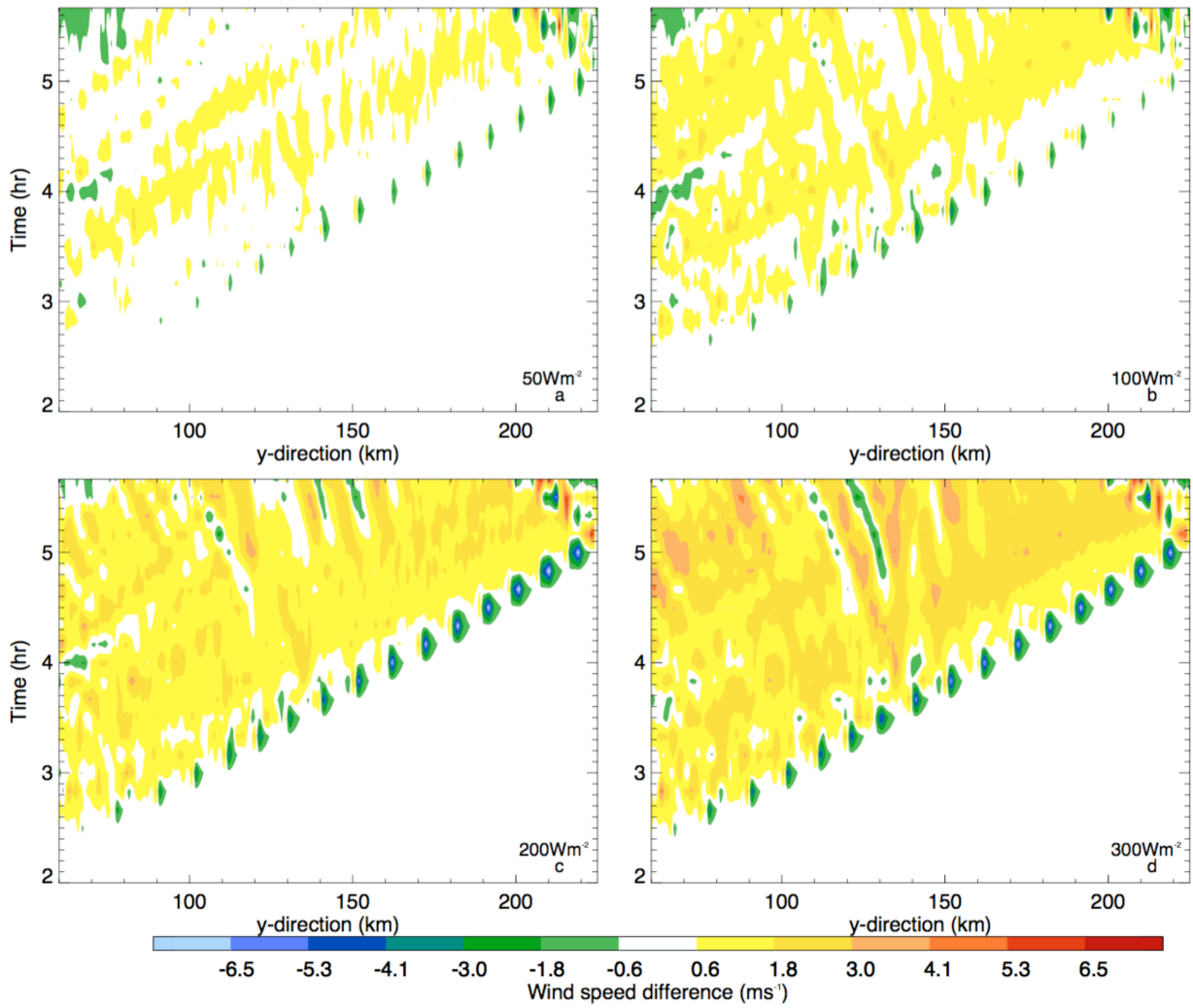

Fig. 9.Hovmöller diagrams of the wind speed difference at the surface layer (0.5 m AGL) for runs with (a) 50 Wm^{-2} (F1), (b) 100 Wm^{-2} (F2), (c) 200 Wm^{-2} (F3) and 300 Wm^{-2} (F4) surface heat flux and the standard run (0 Wm^{-2}, S), respectively.

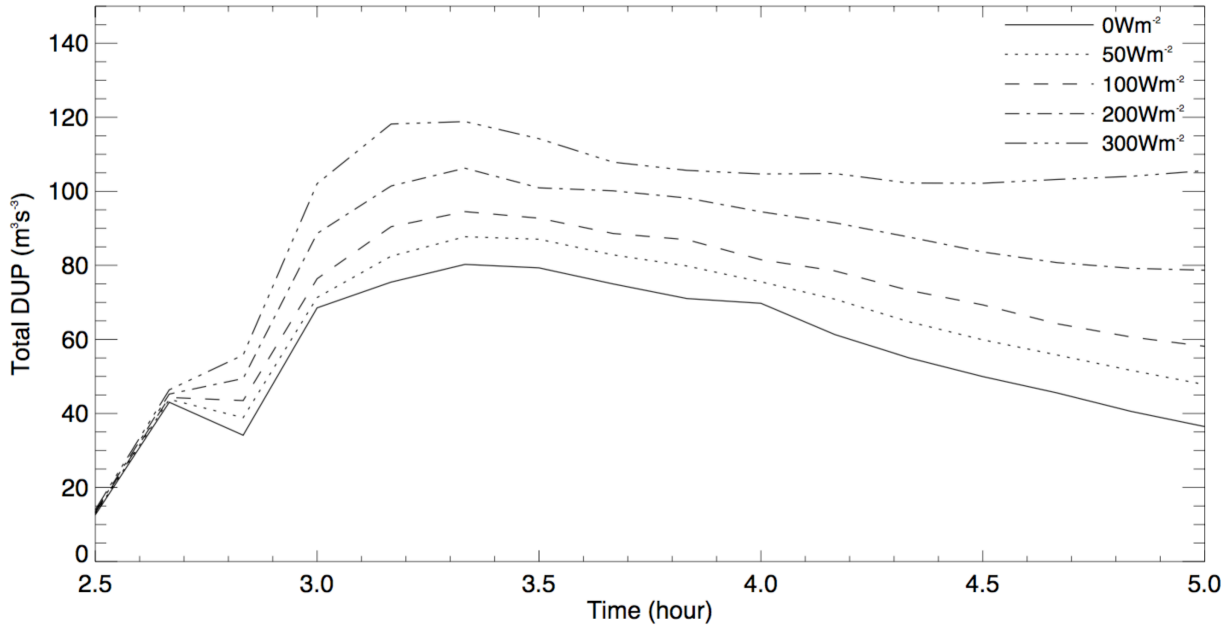

Fig. 10.Total dust uplift potential as a function of time for runs with 0 Wm^{-2} (S), 50 Wm^{-2} (F1), 100 Wm^{-2} (F2), 200 Wm^{-2} (F3) and 300 Wm^{-2} (F4) surface heat flux, respectively.

Table1. Horizontal grid spacing and surface heat fluxes for the sensitivity tests. S is the standard run.

Condition	R1	R2	R3	**S**	R4	R5	R6	R7	R8	F1	F2	F3	F4	S3D
Grid-spacing (km)	0.1	0.2	0.3	**0.45**	0.5	0.6	0.75	0.9	1.0	0.45	0.45	0.45	0.45	0..45
Surface flux (Wm^{-2})	0	0	0	**0**	0	0	0	0	0	50	100	200	300	0

Table 2. Mean propagation speed (ms^{-1}) of cold pools, mean temperature contrast across their leading edges (K), maximum and mean DUPs (m^3s^{-3}) (after 2.0 h) from different resolution runs (R1-R8) and runs with different surface sensible heat fluxes (F1-F4). Mean propagation speeds are estimated from the slope of the leading edge of Hovmöller diagrams of potential temperature. Mean potential temperature differences across leading edge are calculated with the maximum and minimum potential temperatures within 10 kilometers of the leading edge. The leading edge is identified as where dust amount is greater than 0.5 at a height of 120 m.

Condition	R1	R2	R3	**S**	R4	R5	R6	R7	R8	F1	F2	F3	F4	S3D
Propagation speed (ms^{-1})	15.3	16.6	16.0	**16.7**	16.7	18.0	18.2	19.3	23.6	16.9	16.3	15.8	14.8	16.5
Temperature difference (K)	7.6	10.8	12.8	**15.1**	16.7	20.3	20.4	22.5	23.8	15.0	15.0	14.5	14.4	11.5
Max DUP (m^3s^{-3})	6.4	3.4	1.2	**5.0**	2.1	3.1	2.8	3.6	4.3	5.0	4.9	4.7	4.4	5.0
Mean DUP (m^3s^{-3})	0.06	0.08	0.09	**0.11**	0.11	0.11	0.09	0.11	0.11	0.13	0.15	0.18	0.22	0.11